Some Problems Concerning the Accuracy and Efficiency of Self-Consistent Iterative Calculations in Magnetic Recording

H. JANSEN, J. FLUITMAN, AND P. WESSELING

Abstract—There is an increasing interest in the so-called dynamic self-consistent iterative calculations to predict flux reversal patterns in magnetic recording. In the literature one can observe a certain amount of incoherence in the choice of approximations and of numerical methods. The effect of some of the usual approximations are investigated in a systematic way and a new approach in the formulation of the problem is introduced which leads to a considerable gain in efficiency.

I. Introduction

IN SEVERAL PAPERS on the subject of magnetic recording use is made of self-consistent iterative calculations to predict the magnetization pattern or the output voltage of digitally written information. In order to keep such calculations tractable, it is always necessary to accept physical and numerical approximations of the initial problem and an important question is then, of course, how accurate the results are with respect to the exact solution (that cannot be obtained) and, after that, how the results compare with experimental data. Since an exact solution does not exist, one can only reach an insight in the relative accuracy or compare directly with experimental results. In case of deviations it is very difficult then to decide whether the physical model is inaccurate or the numerical methods have been too crude, or both. Even in the case of good looking results, one can feel uneasy about the fact that a happy coincidence of compensating approximations cannot be ruled out. In this study we draw on the work of Portigal [1] and Nishimoto [2], who demonstrated the significance of using accurate hysteresis models, Lindholm [3], who computed the influence of the head gap on the image field, and Bertram [4], who has studied the efficiency of the iteration process.

It is the purpose of this paper to give an overview of the influence of the approximations which are often used and to present a numerical procedure which seems to be more efficient than the methods presented thus far. In Section II we will present our starting points, Section III pays attention to the effect of numerical approximations and Section IV to the effect of approximations in the physical model. Comments and conclusions are the subjects of Section V.

Manuscript received December 12, 1977, revised April 21, 1978.

H. Jansen was with Twente University of Technology, Enschede, The Netherlands. He is now with the Technical Research Department, Netherlands Institute for Fishery Investigation, Ijmuiden, The Netherlands.

J. Fluitman is with Twente University of Technology, Enschede, The Netherlands.

P. Wesseling was with Twente University of Technology, Enschede, The Netherlands. He is now with the Mathematics Department, Delft University of Technology, Delft, The Netherlands.

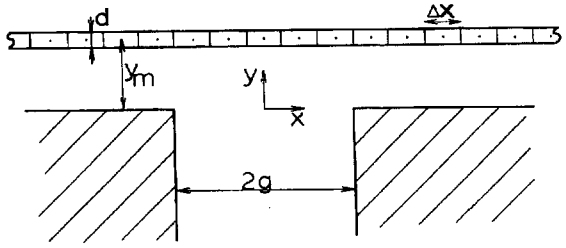

Fig. 1. Head-medium geometry.

II. Starting Points

The problem that has to be solved is mathematically formulated as follows:

$$H(x,t) = H_d(x,M) + H_a(x,t) \tag{1}$$

$$H_d(x,M) = \frac{1}{2\pi}\int_{-\infty}^{+\infty} \frac{dM(\xi)}{d\xi} G(x,\xi)\, d\xi \tag{2}$$

$$M(x) = m(H, \text{history of } H) \tag{3}$$

where x is the coordinate fixed to the recording head (see Fig. 1), t the time, $M(x)$ the magnetization of the medium, H_a the head field, H_d the demagnetizing field, and H the total field. G is the Green function of the problem. Equation (3) is a symbolic expression referring to a hysteresismodel of the material of the recording medium.

The following assumptions are made.

1) The geometry and the material properties are independent of the z-coordinate (z-axis perpendicular on the plane of Fig. 1).
2) Only the x-components of magnetization and magnetic fields are considered.
3) The magnetization is constant over the layer thickness d and its value is equal to the value calculated in the middle of the layer.
4) The recording head material has an infinite permeability.

The influence of these assumptions is not discussed in this paper.

0018-9464/78/1100-1141$00.75

III. Numerical Approximations

Discretization

To transform (1)-(3) into a form suitable for numerical processing, some method of discretization is required. A straightforward way to do so is to divide the medium into segments (of length Δx) and perform calculations in only the center points of the segments (Fig. 1). The functions $H(x)$ and $M(x)$ are thus reduced in discrete vectors, whose components H_j and M_j tell what the values of H and M are in the center of the jth segment. The demagnetizing field H_d can be calculated from the M_j-values by interpolation, differentiation, and solution of (2).

A unified view on the possible interpolation schemes can be developed with the help of sets of basis functions which build up an $M(x)$:

$$M(x) = \sum_i M_i f_i(x) \tag{4}$$

where $f_i(x)$ belongs to a set of basis functions and $\{M_i\}$ is the representation of $M(x)$ with respect to this set. We require that the representation is identical with the one mentioned above where M_j is the value of $M(x)$ at the center of the jth segment. Thus our basis functions must fulfill the requirement

$$M(x_j) = M_j = \sum_i M_i f_i(x_j) \tag{5}$$

which is true for

$$f_i(x_j) = \delta_{ij} \tag{6}$$

where δ_{ij} is the Kronecker delta function.

Two sets of basis functions have been studied: 1) hat functions (Fig. 2(a)) with

$$f_i(x) = f(x - x_i)$$

and

$$f(x) \equiv \begin{cases} 1, & \text{for } -\Delta x/2 < x \leqslant \Delta x/2 \\ 0, & \text{elsewhere} \end{cases} \tag{7}$$

and 2) Hermite splines (Fig. 2(b)) with again

$$f_i(x) = f(x - x_i)$$

but now

$$f(x) \equiv h(x) + \frac{h^*(x - \Delta x) - h^*(x + \Delta x)}{2\Delta x} \tag{8}$$

where

$$h(x) \equiv \begin{cases} 2\left(\frac{|x|}{\Delta x}\right)^3 - 3\left(\frac{|x|}{\Delta x}\right)^2 + 1, & \text{for } |x| < \Delta x \\ 0, & \text{elsewhere} \end{cases}$$

$$h^*(x) \equiv \begin{cases} x\left(1 - \frac{|x|}{\Delta x}\right)^2, & \text{for } |x| < \Delta x \\ 0, & \text{elsewhere.} \end{cases}$$

The description with hat functions is identical with the usual approximation of the integral expression (2) (approximation of differentials by differences and integration by parts). The Hermite splines form an example of a "smooth" interpolation scheme in the expectation that such a scheme might speed convergence and/or reduce the number of mesh points.

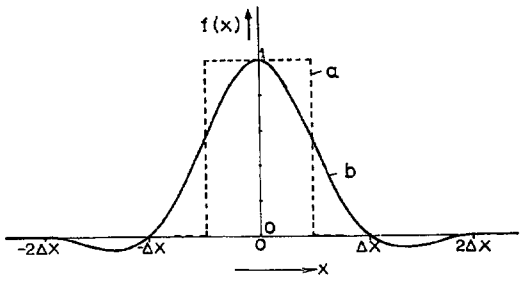

Fig. 2. Basic functions $f(x)$. (a) Hat. (b) Hermite spline.

For significant time reduction the influence of the head-field must be restricted to a finite number of elements ($-n$ to n), and it must also be assumed that the demagnetizing field in any point j is composed of the contributions of only a finite number of neighboring elements ($j - p$ to $j + p$). In general there is no relation between p and n. The formulas (1)-(3) are transformed now to a set of matrix formulae

$$H = H_d + H_a \tag{1'}$$

$$H_d = A \cdot M \tag{2'}$$

$$M_i = \begin{cases} m(H_i, \text{history}_i), & |i| \leqslant n \\ M_i^{(0)}, & n < |i| \leqslant n + p \end{cases} \tag{3'}$$

where $M_i^{(0)}$ is the starting value of M_i, and H, M, and A represent matrices of the form

$$\begin{bmatrix} H_{-n} \\ \cdots \\ \cdots \\ \cdots \\ H_{+n} \end{bmatrix}, \quad \begin{bmatrix} M_{-n-p} \\ \cdots \\ \cdots \\ \cdots \\ \cdots \\ \cdots \\ M_{+n+p} \end{bmatrix}, \text{ and } \begin{bmatrix} A_{-n,-n-p} & \cdots & A_{-n,+n+p} \\ \cdots & \cdots & \cdots \\ \cdots & \cdots & \cdots \\ \cdots & \cdots & \cdots \\ \cdots & \cdots & \cdots \\ \cdots & \cdots & \cdots \\ A_{+n,-n-p} & \cdots & A_{+n,+n+p} \end{bmatrix}$$

respectively. The elements of A are given by

$$A_{ij} \equiv \begin{cases} \frac{1}{2\pi}\int_{-\infty}^{+\infty} G(x_i, \xi)\frac{df_j(\xi)}{d\xi}\,d\xi, & |i - j| \leqslant p \\ 0, & |i - j| > p. \end{cases} \tag{9}$$

The interpolation scheme and the values of Δx, n, and p are determined from the criterion that the error in M is within 1 percent of the saturation magnetization. Generally, an exact solution is unknown so that a variation of $\Delta x, n$, and p must give information whether or not the result is close enough to the limiting case with $\Delta x \to 0$ and $n\Delta x, p\Delta x \to \infty$. There is one representative case, however, which can be solved analytically.

This test case is described by van Herk and Wesseling [5] and refers to the situation that (3) is reduced to

$$M = M_r(H/H_c - 1)$$

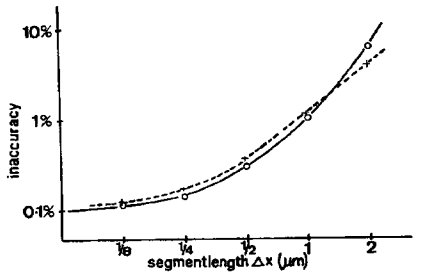

Fig. 3. Inaccuracy versus segment length for the basis functions hat (+) and Hermite spline (○) for the testcase with $d = 1$ μm, $y_m = 1$ μm, $2g = 3$ μm, $M_r = 2.4H_c$, $n = p = 20$ μm/Δx. The inaccuracy is related to the amplitude of M (inaccuracy = magnetization error divided by $(M_{max} - M_{min})/2$). The remaining error for $\Delta x \to 0$ is caused by the fact that n and p are not infinite.

with M_r and H_c constants, and G is approximated by

$$G = d/(\xi - x)$$

with d the medium thickness. Furthermore, the Karlquist field is used for the head field. Although the physical approximations are rather severe in this case, it can be used without hesitation to test the accuracy of numerical methods and approximations. A complete test has been performed with $d = y_m = 1$ μm, $2g = 3$ μm, $M_r = 2.4H_c$, and $n = p = 20$ μm/Δx (symbols explained in Fig. 1). In Fig. 3 the deviation of the computed results from the exact solution is displayed as a function of Δx, the segment length. In this case n and p are chosen sufficiently large to cause only a negligible error (0.1 percent for $\Delta x \to 0$). It is seen that the choice of the basis functions to represent $M(x)$ is of minor importance for the accuracy (as it proved to be with respect to the efficiency) and segment lengths up to about 1 μm (so n and p values of about 20) can be used for this case. In this way an indication of the error due to the discretization procedure can be obtained in all cases.

In the course of our work we have felt the need of some standard situation in order to be able to compare our results with the work of other authors. Therefore, we have chosen the patterns described by Nishimoto *et al.* [2] characterized by $M_i^{(0)}/M_s = 0.85$ (premagnetized state), $M_s = 800\,000$A/m, $H_c = 56\,000$A/m, $H_0 = 320\,000$A/m, $d = 0.05$ μm, $y_m = 0.325$ μm, and $2g = 1$ μm. Following the procedure outlined above, the error due to discretization proved to be smaller than 1 percent, for the choice $\Delta x = 0.125$ μm, $n = 30, p = 15$. Unless stated otherwise, this characteristic case is used throughout the paper.

Approximation of the Green Function

The Green function $G(x, \xi)$ and the fringe field $H_a(x, t)$ can be computed exactly by conformal mapping. Mostly, G and H_a are approximated by neglecting the head gap in the image field and assuming the magnetic potential to vary linearly across the head gap (Karlquist approximation). G and H_a can then be expressed as follows:

$$G(x, \xi) \cong G_k(x, \xi) \equiv 2 \arctan \frac{d/2}{\xi - x} - \arctan \frac{2y_m + d/2}{\xi - x} + \arctan \frac{2y_m - d/2}{\xi - x} \tag{10}$$

$$H_a(x, t) \cong H_{ak}(x, t) \equiv \frac{H_0(t)}{\pi} \left(\arctan \frac{g + x}{y_m} + \arctan \frac{g - x}{y_m} \right) \tag{11}$$

where H_0 is the deep gap field, y_m the distance between the head and the center of the medium, and d the layer thickness. Sometimes G_k is simplified further as follows:

$$G_k(x, \xi) \cong G_{ka}(x, \xi) \equiv \frac{d}{\xi - x} - \frac{d(\xi - x)}{(\xi - x)^2 + 4y_m^2} \tag{12}$$

where the index a denotes the fact that the arctan is approximated by its argument.

To evaluate the effect of approximating $G(x, \xi)$ by $G_k(x, \xi)$, i.e., ignoring the head gap, we consider the matrix A as defined in (9) but now written as

$$A_{ij} = (A_{ij})_k + \Delta_{ij}$$

with

$$(A_{ij})_k = \frac{1}{2\pi} \int_{-\infty}^{+\infty} G_k(x_i, \xi) \frac{\partial f(\xi - x_j)}{\partial \xi} d\xi.$$

Here Δ_{ij} can be considered as representing the gap influence.

We have studied the effect of omission of Δ_{ij} on the resulting $M(x)$ and have found that the error made does not exceed 1 percent of M_s, even in a case for which $2g/y_m = 10$. So, notwithstanding the influence of the presence of the gap on the image field, as shown by Lindholm [3] the effect on the write process is negligible. This can be made plausible when it is realized that in front of the gap where the influence of the approximation is expected to be large the medium is always driven into saturation.

Sometimes it is seen that G_k is approximated by G_{ka} (12). This approximation only has disadvantages. A_k or A_{ka} has only to be computed once so there is hardly a gain in computing time while the influence on the results may be considerable for relatively thick layers (see Fig. 4). The error increases with the medium thickness and with the bit density.

Method of Iteration

In the literature the following iteration procedure is mostly used:

$$H^{(k+1)} = H^{(k)} + \beta \cdot (H_d^{(k+1)} - H^{(k)} + H_a) \tag{13}$$

with β a relaxation parameter matrix and k the number of the iteration step. $H_d^{(k+1)}$ is computed from $M = m(H^{(k)}$ history).

An attractive alternative is the second-order iteration procedure according to Newton-Raphson from which is derived (see Appendix I):

$$(1 - A' \cdot \Lambda^{(k)}) \cdot (H^{(k+1)} - H^{(k)}) = H_d^{(k+1)} - H^{(k)} + H_a. \tag{14}$$

Here 1 is the identity matrix, A' is derived from A by omitting the columns $-n - p$ to $-n - 1$ and $n + 1$ to $n + p$, and $\Lambda^{(k)}$ is the diagonal matrix with elements dM/dH, evaluated from the hysteresis model at H_i, M_i. Equation (13) can be transformed

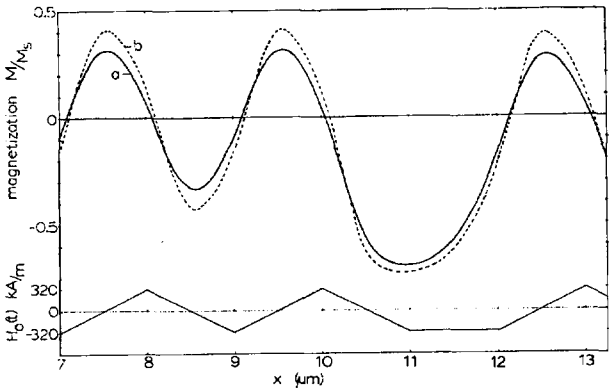

Fig. 4. Influence of approximating the arctan by its argument for a bit density of 10^6 bits/m and hysteresis curve II (see Fig. 6). (a) Approximated Green function G_{ka} for all layer thicknesses d with $M_s * d = 0.04$ A. (b) Not-approximated Green function G_k, $M_s = 80\,000$A/m, $d = 0.5$ μm. N.B. Only part of the pattern is shown here (as is the case for Fig. 7 and 8 as well). In the full computation $H_0(t)$ is taken periodic (in the way depicted from $x = 7$ to $x = 11$ μm) for $x = -1$ to $x = 11$ μm, and from $x = 12$ to $x = 18$ μm.

into (14) by putting

$$\beta = (1 - A' \cdot \Lambda^{(k)})^{-1} \tag{15}$$

and our set of basis functions which yields A now leads to a simple expression for an optimal relaxation factor. Very fast (second order) convergence can be obtained with this method, once the result is close enough to the final result. A disadvantage may be that it can take several steps before the Newton process starts to show second-order convergence. Bertram [4] has suggested an iterative method which can be formulated similar to (14) except for Λ, which is not taken to be dM/dH. In his paper the method is described for a simple MH-curve, going through the origin. In that case $\Lambda_{ii}^{(k)}$ is replaced by $\chi_{ii}^{(k)}$:

$$\chi_{ii}^{(k)} = M_i^{(k)}/H_i^{(k)}$$

but this idea can be extended for an arbitrary hysteresis curve so that we have

$$\chi_{ii}^{(k)} = \frac{M_i^{(k)} - M_i^{(0)}}{H_i^{(k)} - H_i^{(0)}}.$$

Applying this formula for $\Lambda_{ii}^{(k)}$ has the advantage that in the first stage of the iteration convergence is faster, but when second-order convergence sets in Bertram's method is considerably slower. It goes without saying that an alternative which combines both methods is promising, and therefore we have studied the procedure derived from the Newton-Raphson process (14) but taking $\psi_{ii}^{(k)}$ instead of $\Lambda_{ii}^{(k)}$ where

$$\psi_{ii}^{(k)} = \begin{cases} \dfrac{M_i^{(k)} - M_i^{(k-1)}}{H_i^{(k)} - H_i^{(k-1)}}, & \text{for } k > 0 \\ \dfrac{M_s}{H_c}, & \text{for } k = 0. \end{cases} \tag{16}$$

In doing so the process starts in the way proposed by Bertram (second step) and then gradually transforms into the Newton process. This results in a general increase of the efficiency as is demonstrated in Table I.

TABLE I

NUMBER OF ITERATION STEPS NEEDED FOR DIFFERENT METHODS (CPU-TIME PER STEP IS EQUAL FOR ALL CASES) FOR THE CASE MENTIONED IN THE TEXT (EXCEPT $d = 0.15$ μm AND $p = 30$) WITH $b = 11$. ITERATION WAS STOPPED WHEN $|H_i^{(k+1)} - H_i^{(k)}|_{max} < 10^{-6} H_c$

	Iteration method		
hysteresis curve (see figure 6)	Newton Λ	Bertram X	Combined Ψ
I	Divergence	Divergence	13
II	11	36	9
III	12	> 50	11

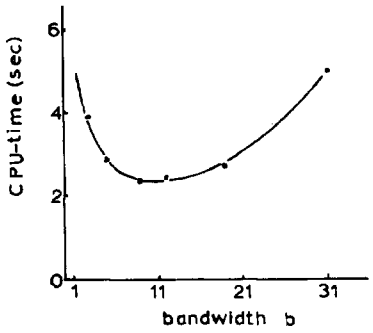

Fig. 5. CPU-time versus bandwidth b for the case mentioned in the text and hysteresis curve II, iteration stopped when $|H_i^{(k+1)} - H_i^{(k)}|_{max} < 10^{-6} * H_c$. (Maximum bandwidth is $2p + 1$.)

Another point of interest is the possibility to change the matrix A'. A change of A' is of no influence on the accuracy of the final result (as long as there is convergence) but influences the rate of convergence. We have studied the effect of a transformation of A' into a bandmatrix of bandwidth b (all elements outside a band around the diagonal are set equal to zero). Since each iteration step requires the solution of a set of linear equations with matrix $1 - A' \cdot \Lambda^{(k)}$, reduction of A' in the above sense may result in a gain in CPU-time which is larger than the accompanying loss caused by an increasing number of iteration steps. This is shown in Fig. 5. The CPU time is determined by the strict convergence criterion, the complex hysteresis model and the detailed intermediate printout we have used in our computations (carried out on a DEC system 10 computer).

The Write and Read Process

It is assumed that the magnetization follows the driving fields instantaneously, so that (1)–(3) describe the magnetization properly in the dynamic case as well. A justification of this assumption can be found in the literature [6]. A complete write operation involves a number of iterations with the lateral head/medium position shifted continually over discrete intervals, for instance of length Δx. When the magnetization is coming out of the range of the head field, the pattern must be recalculated while removing the image to simulate the re-

moved head situation. Reading can be simulated by first recalculating M in the presence of image fields from the read head and then calculate the readback voltage utilizing the reciprocity theorem.

The choice of the length of the shift intervals is important in order to simulate the dynamic process correctly. It is tempting to choose this interval equal to Δx but this is sometimes inaccurate, sometimes inefficient. We will analyze the situation by considering linear transitions (with transition time T).

For small values of T, i.e., for $vT \leq 2|H_a/(dH_a/dx)|_{\min}$, all layer segments will experience a headfield that increases or decreases (depending on the polarity of the reversal) monotonously during the reversal (the proof is in Appendix III). If the same holds for the total field H (and this can be proven, see Appendix II) then there is no need to carry out intermediate calculations during the reversal, because the magnetization in any segment remains on one minor loop, from the start to the end of the reversal. So we can conclude that it is inefficient to maintain a shift interval Δx, when $\Delta x < vT \leq 2|H_a/(\partial H_a/\partial x)|_{\min}$. In the case that $vT > 2|H_a/(\partial H_a/\partial x)|_{\min}$ there are field extrema, felt by the medium, during the transition. Generally, $|H_a/(\partial H_a/\partial x)|_{\min}$ is larger than Δx so that shifting over Δx may give good results. In that case it must be checked whether the error is tolerable or not. When $|H_a/(\partial H_a/\partial x)|_{\min} \leq \Delta x$ it is necessary to reduce the shift intervals to values smaller than Δx.

In the calculation of the magnetization patterns of Figs. 4, 7, and 8 the "small rise time criterion" mentioned above is fulfilled, so computations are only carried out at the start (end) of a headfield transition. However, in the interval without a transition (interval 11-12 μm) the shift must be much smaller and is taken to be equal to the segment length ($\Delta x = 0.125$ μm in our case). Figs. 4, 7, and 8 display only a part of the computed patterns (see caption to Fig. 4).

We have recalculated the patterns on removing the head ($y_m \to \infty$). In this process the mirror images disappear and we have found that there are occasions when segments experience a field extremum during this process so that a gradual (stepwise) removal should be simulated rather than a removal in one step. However, this effect is probably of minor importance and in fact we have found no difference in the results whether, for the patterns of Figs. 4, 7, and 8, the removal was simulated in one step or in several steps. The same remarks are valid for the opposite case when the head returns to its original position.

IV. Physical Approximations

Hysteresis Model

For the hysteresis loop $m(H, \text{history})$ we use the model devised by Fluitman and Uilhoorn [7] which can be seen as an extended combination of the major loop model of Mazières and Fourquet [8] and the minor loop description of Nishimoto [2]. The major loop in the first quadrant is expressed by the formula

$$(M_s - M)(H/H_c - rM/M_s - 1) = qM \tag{17}$$

where M_s is the saturation magnetization, r a parameter to express the shear of the loop, and q a curvature parameter.

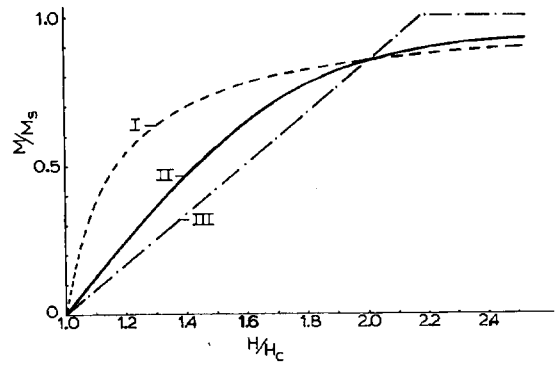

Fig. 6. The first quadrant of (I): a square looking ($r = 10^{-4}, q = 0.1765$), (II): a Potter and Schmulian like ($r = 0.75$, $q = 0.064$), and (III): a sheared ($r = 1.178$, $q = 10^{-4}$) hysteresis curve (parameters from eq. (17)). (N.B. The M/M_s-axis is not drawn at the origin of the H/H_c-axis, but at $H/H_c = 1$!)

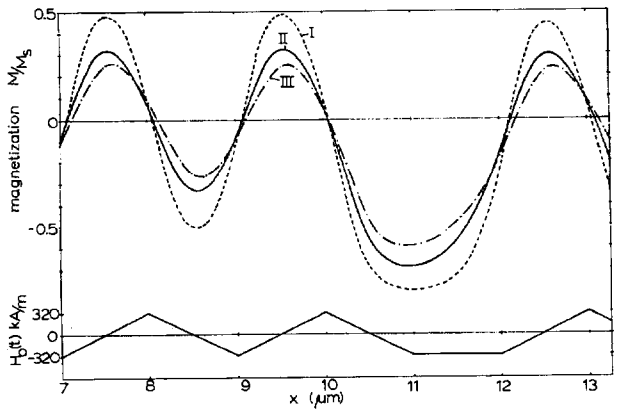

Fig. 7. Magnetization calculated with (I) a square looking, (II) a Potter and Schmulian like, and (III) a sheared hysteresis model at a bit density of 10^6 bits/m. Other parameters are as mentioned in the text.

Minor loops of any order are derived from this hyperbolic major loop by a geometrical multiplication process, and they reflect the characteristics of the major loop. The derivations of the minor loops is analogous to the procedure of Nishimoto *et al.* with the extension that the geometrical direction of the multiplication is another free parameter to fit to actual hysteresisloops. The details are in [7]. The model is more accurate than preceding models and flexible enough to represent, by proper choice of the parameters, the more simple models of Potter and Schmulian [9] or of Tjaden and Tercic [10], for instance. So this model is very suitable for studying the effect of accurate modeling.

We have performed the following test. A choice was made of the parameters M_s and H_c, we put $M_r = 0.85\ M_s$, and then the remaining parameters in (17) were chosen in such a way that we had a square-looking, a Potter-Schmulian-like, and a sheared major loop (Fig. 6). Using these curves in the calculations led to results which differ drastically among each other (Fig. 7). So a proper choice is very important. But this immediately draws the attention to the question whether the "bulk" hysteresis curve, taken from samples cut from tapes

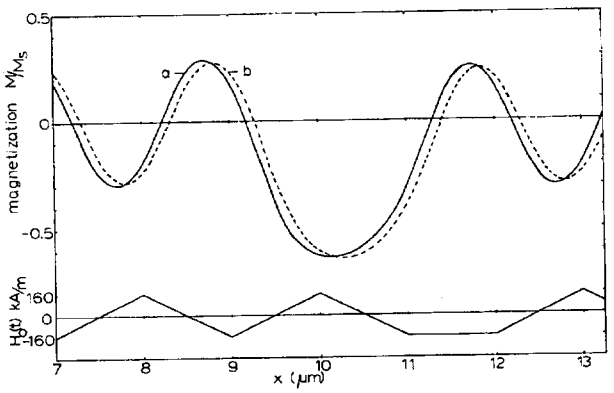

Fig. 8. Magnetization calculated with (a) exact and (b) Karlquist head field. Parameters as mentioned in the text (except $2g = 3$ μm, $H_0 = 160\,000$A/m), hysteresis curve II.

or disks, represents the effective hysteresis on a microscale. We have misgivings concerning the accuracy of calculations, even if the results look trustworthy, if the hysteresis model does not closely conform to reality.

Head Fields

For the headfield the Karlquist approximation H_{ak} (11) may be used instead of H_a as long as $2g/y_m < 4$. But even for larger values of $2g/y_m$ the errors are small, as is shown in Fig. 8 for the extreme situation $2g/y_m = 10$. Another point is whether the experimental head field of the micro-ferrite heads in disk drives do indeed have an appearance like H_a. Reliable experimental data are needed, but for the time being we have some doubt (as in the case of the choice of hysteresis model) about the appreciation of apparently good results of computations relying on the Karlquist field.

V. Conclusions

We have studied the effect of a number of measures and approximations in the calculation of one-dimensional magnetization patterns. A unified method in defining approximated $M(x)$ functions has been introduced to treat the problem in a systematic way. Errors resulting from discretization have been calculated by comparison with analytic results and have been shown to be small, if the right precautions are taken. The influence of the gap on the image field was found to be negligible. Approximating arctan functions by their arguments (in the Green function) may lead to unnecessarily large errors. A procedure of iteration, derived from the Newton-Raphson method, has been introduced which results in a reduction of CPU-time. The influence of the choice of a hysteresis model was found to be important and the attention has been drawn to the necessity of investigating the hysteresis or the particle interaction model on a microscale as well as the structure of head fields of practical recording heads.

Appendix I

Substitution of (2′) and (1′) leads to

$$H = A \cdot M + H_a. \tag{18}$$

$A \cdot M$ is rewritten as $A' \cdot M' + A'' \cdot M''$ where A' is the $(n * n)$ matrix which results from A by omitting the columns $-n - p$ to $-n - 1$ and $+n + 1$ to $+n + p$, and M' is the $(n * 1)$-vector derived from M by omitting the components M_{-n-p} to M_{-n-1} and M_{+n+1} to M_{+n+p}. A'' is derived from A by putting all $A_{ij} = 0$ for $|i|, |j| \leqslant n$, and M'' is derived from M by putting $M_i = 0$ for $|i| \leqslant n$. One obtains

$$H = A' \cdot M' + A'' \cdot M'' + H_a. \tag{19}$$

$A'' \cdot M''$ is the contribution to H_d from the magnetic charges outside the computation region, and this contribution remains constant during the iteration. To solve (19) is to find the zero of

$$G(H) = H - H_a - A' \cdot M' - A'' \cdot M'' \tag{20}$$

or, with the help of (3′),

$$G(H) = H - H_a - A' \cdot m(H, \text{history}) - A'' \cdot M''. \tag{21}$$

Let H^* be the solution of $G(H) = 0$, then, using Taylor's series, we have as a first approximation

$$DG(H) \cdot (H^* - H) = -G(H). \tag{22}$$

$DG(H)$ is found by differentiating (21)

$$DG(H) = 1 - A' \cdot \Lambda \tag{23}$$

with $\Lambda_{ii} = (dm/dH)|_{H_i}$, $\Lambda_{ij} = 0$, $i \neq j$. From (22) and (23) the iteration can be derived:

$$(1 - A' \cdot \Lambda)(H^{(k+1)} - H^{(k)}) = -G(H^{(k)}). \tag{24}$$

Appendix II

It can be shown that, if $\Delta H_{a_i} > 0 (< 0)$ for all i, then $\Delta H_i > 0 (< 0)$ for all i. The proof relies on some properties, which are valid for the matrix A in the case of the representation with hat functions (and neglecting the influence of the head gap):

$$A_{j,i} = A_{i,j} > 0 (i \neq j), A_{i,i} < 0 \text{ and } \sum_{j=-n}^{n} A_{i,j} < 0.$$

The last property is a consequence of the fact that the demagnetizing field is zero when the magnetization is a constant everywhere. Then $H_d = A \cdot M = 0$ or $\Sigma_j A_{i,j} M_j = 0$ or, since M_j is constant, $\Sigma_j A_{i,j} = 0$. The matrix we use is a truncated one with j from $-n$ to n, so $\Sigma_{j=-n}^{n} A_{i,j} < 0$ since only positive terms are neglected in the approximation. From (19) it follows $\Delta H = A' \cdot \Delta M' + A'' \cdot \Delta M'' + \Delta H_a$. Since $\Delta M'' = 0$ (outside computation region), it follows that $\Delta H = A' \cdot \Delta M' + \Delta H_a$ or with $\Delta M = \Lambda \Delta H$

$$(1 - A' \cdot \Lambda)\, \Delta H = \Delta H_a. \tag{25}$$

Suppose now that $\Delta H_{a_i} > 0$ for all i; then we must show that $\Delta H_i > 0$ (all i). Suppose that the latter is not true and that there is a set of i-values $(i_p: p = 1, \cdots, m)$ with $\Delta H_{i_p} < 0$. From (25) we select equations with index i_p for which the general expression reads

$$-A_{i_p,-n}\Lambda_{-n,-n}\Delta H_{-n} \cdots + (1/\Lambda_{i_p,i_p} - A_{i_p,i_p})\Lambda_{i_p,i_p}\Delta H_{i_p} \cdots - A_{i_p,n}\Lambda_{n,n}\Delta H_n = \Delta H_{a_{i_p}}. \tag{26}$$

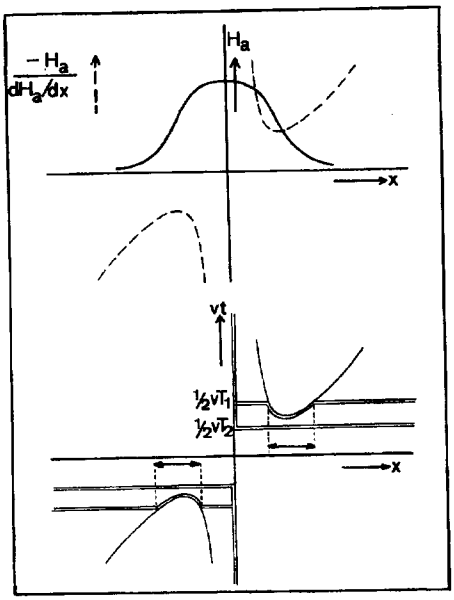

Fig. 9. (a) Head field H_a (drawn) and $-H_a/(dH_a/dx)$ (-----) as a function of x. (b) Set of (x, t)-values for which there is an extremum at $x_m = x - vt$ (double drawn curves). Two situations are indicated. In the case $T = T_2$ there will be no particle in the layer experiencing a field extremum during the transition (extremum may occur at edge $t = \frac{1}{2} T_2$).

Since $\Lambda_{i,i} > 0$, for all i, all terms on the left side with column index $i \neq i_p$ are negative since $\Delta H_i > 0$, for $i \neq i_p$. When all these terms are transported to the right side, the right side only consists of positive terms which means that the remainder on the left side must be positive as well. So we arrive at a set of m inequalities which can be denoted as follows:

$$\begin{aligned}
(1/\Lambda_{i_1,i_1} - A_{i_1,i_1})\,\Lambda_{i_1,i_1}\Delta H_{i_1} - \cdots \quad & -A_{i_1,i_p}\Lambda_{i_p,i_p}\Delta H_{i_p} > 0 \\
\cdots\cdots\cdots\cdots\cdots\cdots \quad & \cdots\cdots\cdots\cdots\cdots\cdots > 0 \\
-A_{i_p,i_1}\Lambda_{i_1,i_1}\Delta H_{i_1} \quad & \cdots (1/\Lambda_{i_p,i_p} - A_{i_p,i_p})\,\Lambda_{i_p,i_p}\Delta H_{i_p} > 0. \qquad (27)
\end{aligned}$$

Since the sum of all terms are positive in each inequality the same must be true for the total sum of all terms together.

Let us now consider the summation of all terms in another order, namely, column for column. The first column of terms in (27) gives

$$\{(1/\Lambda_{i_1,i_1} - A_{i_1,i_1}) - A_{i_2,i_1} \cdots - A_{i_p,i_1}\}\,\Lambda_{i_1,i_1}\Delta H_{i_1}. \quad (28)$$

Since $\Sigma_{j=-n}^{n} A_{j,i} < 0$ it follows that $\Sigma_{p=1}^{m} A_{i_p,i} < 0$ (again only positive terms are left out). Together with $\Delta H_{i_1} < 0$ and $\Lambda_{i_1,i_1} > 0$ this gives a negative result. The same is true for all columns, of course, so that we now find that an addition of all terms in (27) gives a negative result in contradiction with the foregoing. So the supposition that there are $\Delta H_{i_p} < 0$ leads to a contradiction and this proves that $\Delta H_i > 0$ for all i.

Appendix III

The extreme fields, experienced by a particle moving through a time-dependent head field, are calculated by setting the time derivative of $H_a = H_a(x)f(t)$ equal to zero under the condition that x_m is a constant. Here x_m is the particle coordinate with respect to the medium (remember that x is the particle coordinate with respect to the head, so we have $x_m = x - vt$ with v the lateral head/medium velocity). From this it follows that

$$\frac{1}{H_a}\frac{dH_a}{dx} = -\frac{1}{f}\frac{df}{dt}\frac{1}{v}. \qquad (29)$$

In the case of a linear transition with rise time T, (29) transforms into

$$\begin{aligned}
&\frac{1}{H_a}\frac{dH_a}{dx} = -\frac{1}{vt}, \qquad -\frac{1}{2}T < t < \frac{1}{2}T \\
&\frac{1}{H_a}\frac{dH_a}{dx} = 0, \qquad |t| > \frac{1}{2}T. \qquad (30)
\end{aligned}$$

In Fig. 9(a), $-H_a/(dH_a/dx)$ is given as a function of x. Since (30) is valid, the ordinate equals vt for $-\frac{1}{2}T < t < \frac{1}{2}T$, while for $|t| > \frac{1}{2}T$, $(1/H_a)\,(dH_a/dx) = 0$, which can only be true for $x = 0$. For x-values outside the indicated interval in Fig. 9(b) and $x \neq 0$, the extreme field values are reached neither inside nor outside the transition but exactly at the edge $t = \frac{1}{2}T$ (boundary extreme). So with these elements the set of (x, t)-values, for which an extremum appears, is complete (double lines in Fig. 9(b)). It is immediately clear that there will be no extremum during the transition as long as $vT/2 \leq |H_a/(dH_a/dx)|_{\min}$ ($T = T_2$ in Fig. 9(b); extremum may occur at edge $t = \frac{1}{2} T_2$). When $vT/2 > |H_a/(dH_a/dx)|_{\min}$ there are extrema in the intervals indicated in the figure ($T = T_1$). This case is completely worked out in [11].

Acknowledgment

The paper is the result of the combined efforts not only of the three authors but also of Ir. B. de Boer and Ir. A. den Ouden who contributed via their master's work in an earlier stage of the project. In some stages the work was also supported by Ir. A. van Herk and Ir. R. Moot.

References

[1] D. L. Portigal, "A magnetic recording simulation program having an improved fit to actual hysteresis loops," IEEE Trans. Magn., vol. MAG-11, pp. 934-941, May 1975.

[2] K. Nishimoto, M. Nagao, Y. Suganuma and H. Tanaka, "Computer simulations of high-density multiple transitions in magnetic disc recording," IEEE Trans. Magn., vol. MAG-10, pp. 769-773, Sep. 1974.

[3] D. A. Lindholm, "Image fields for two-dimensional recording heads," IEEE Trans. Magn., vol. MAG-13, pp. 1463-1465, Sep. 1977.

[4] H. N. Bertram, "On the convergence of iterative solutions of the integral magnetic field equation," IEEE Trans. Magn., vol. MAG-11, pp. 928-933, May 1975.

[5] A. van Herk and P. Wesseling, "An analytical model of the write and read process in digital recording with a "linear" recording medium," Trans. Magn., vol. MAG-10, pp. 761-764, Sep. 1974.

[6] R. F. M. Thornley and J. A. Williams, "Switching speeds in magnetic tapes," IBM J. Res. Develop., vol. 18, pp. 576-578, Nov. 1974.

[7] J. H. J. Fluitman and F. W. Uilhoorn, "A mathematical model for simulating the hysteretic behavior of magnetic materials," J. Appl. Sci. and Engin. A, vol. 2, pp. 107-116, June 1977.

[8] C. Maizières and M. Fourquet, "Simulations d'une bobine à noyau de fer par représentation mathématique du cycle d'hysteresis," Revue Generale de l'Electricité, vol. 77, pp. 873–880, Dec. 1971.
[9] R. I. Potter and R. J. Schmulian, "Self-consistently computed magnetization patterns in thin magnetic recording media," IEEE Trans. Magn., vol. MAG-7, pp. 873–880, Dec. 1971.
[10] D. L. A. Tjaden and E. J. Tercic, "Theoretical and experimental investigations of digital magnetic recording on thin media," Philips Res. Rep., vol. 30, pp. 120–161, 1975.
[11] J. Fluitman, "Effect of nonzero write field rise time in digital magnetic recording," IEEE Trans. Magn., vol. MAG-12, pp. 218–223, May 1976.

Magnetic Traction Force in an HGMS with an Ordered Array of Wires: I

ITAMAR EISENSTEIN

Abstract—**The magnetic traction force, experienced by a paramagnetic sphere inside an infinite ordered array of wires that forms the matrix of an HGMS, is calculated. A comparison is made, for a particular case, with the forces (exact and approximate) due to a single wire and to two wires. It is found that the single wire forces are reasonably good approximations for high applied fields and small filling factors provided they are made to vanish midway between two adjacent wires.**

I. Introduction

THE SEPARATING medium in a high-gradient magnetic separator (HGMS) contains a ferromagnetic matrix that consists of a large number of filamentary wires. Still, theoretical treatments of such separators rely on models that involve one wire only. This is comprehensible in view of the difficulty in treating the availing "chaotic" matrices such as stainless steel wool. Recently, however, matrices that consist of an ordered array of wires were considered [1]–[3] and proved to be more promising than the disordered ones. Ordered matrices are more easily accessible to a theoretical treatment and, accordingly, it is the aim of this paper to treat the magnetostatics of such a matrix. Actually, we shall consider an *infinite* ordered array of wires and shall calculate the magnetic force experienced by a paramagnetic particle inside the array. Such an infinite array is often a good approximation to an actual finite one and should point at qualitative differences between a many-wires-matrix and a single wire. The magnetic force in the array involves an infinite lattice sum over the field contributions of the individual wires. For an arbitrary position of the paramagnetic particle this sum cannot be reduced to a single-term expression and should be evaluated numerically. The problem is that the convergence is very slow and the result depends on the order of summation. The first difficulty is treated by using a lattice sum technique that converts the original sum into a rapidly convergent one. The second difficulty is treated by assigning a physical significance to the order of summation. The resulting magnetic force is calculated numerically and compared with computations pertinent to a single wire.

Manuscript received August 19, 1977; revised March 30, 1978.
The author is with the Department of Electronics, Weizmann Institute of Science, Rehovot, Israel.

II. Preliminaries

We consider an infinite array of parallel ferromagnetic wires that lie along the z-axis. Each wire is infinitely long, it has a circular cross section with a radius a, and it is saturated to a magnetization M along the x axis by an external field H_0 along the same axis. The cross section of the array in the $x-y$ plane forms a simple rectangular lattice with lattice constants a_1 and a_2 along the x and y axes, respectively (Fig. 1).

Consider now a paramagnetic sphere with a radius b inside the array (Fig. 2). Choose the $z = 0$ plane to pass through the center of the sphere (which, due to the independence on z, involves no loss in generality) with the origin of coordinates on the axis of a wire. Let R be the distance of the center of the sphere from the origin and Φ_0 the angle between the x axis and the direction along which R is measured. Let H be the total magnetic field in the array and U the corresponding magnetostatic potential:

$$H = -\nabla U = -\nabla (U_0 + U_1) \tag{1}$$

where U_0 is the magnetostatic potential due to H_0,

$$U_0 = -H_0 x \tag{2}$$

and U_1 is the magnetostatic potential due to the lattice magnetization. The magnetic energy of the paramagnetic sphere is

$$E = -\tfrac{1}{2} (\chi_p - \chi_m) \int (\nabla U)^2 \, dv \tag{3}$$

where χ_p and χ_m are the susceptibilities of the paramagnetic sphere and the inter-wire medium, respectively, and the inte-

0018-9464/78/1100-1148$00.75